

## Article

# Modulatory Impact of Tefluthrin, Telmisartan, and KB-R7943 on Voltage-Gated Na<sup>+</sup> Currents

Hsun-Yu Huang <sup>1,†</sup> , Yi-Bo Huang <sup>2,†</sup>, Chao-Liang Wu <sup>3</sup>  and Sheng-Nan Wu <sup>4,5,6,\*</sup> 

<sup>1</sup> Department of Dentistry, Ditmanson Medical Foundation Chia-Yi Christian Hospital, Chiayi City 60002, Taiwan; 07114@cych.org.tw

<sup>2</sup> Department of Stomatology, Ditmanson Medical Foundation Chia-Yi Christian Hospital, Chiayi City 60002, Taiwan; 07318@cych.org.tw

<sup>3</sup> Department of Medical Research, Ditmanson Medical Foundation Chia-Yi Christian Hospital, Chiayi City 60002, Taiwan; wumolbio@mail.ncku.edu.tw

<sup>4</sup> Department of Research and Education, An Nan Hospital, China Medical University, No. 66, Section 2, Changhe Road, An Nan District, Tainan 70965, Taiwan

<sup>5</sup> School of Medicine, College of Medicine, National Sun Yat-sen University, Kaohsiung 80424, Taiwan

<sup>6</sup> Department of Physiology, College of Medicine, National Cheng Kung University, Tainan 70101, Taiwan

\* Correspondence: 071320@tool.caaumed.org.tw or snwu@mail.ncku.edu.tw; Tel.: +886-6-3553111-3657

† These authors contributed equally to this work.

**Abstract:** Tefluthrin (Tef) is categorized as a type-I pyrethroid insecticide, telmisartan (Tel) functions as an angiotensin II receptor blocker, and KB-R7943 has been identified as an inhibitor of the Na<sup>+</sup>-Ca<sup>2+</sup> exchange process. However, the influence of these compounds on the amplitude and gating properties of voltage-gated Na<sup>+</sup> current ( $I_{Na}$ ) in neurons associated with pain signaling remains unclear. In cultured dorsal root ganglion (DRG) neurons, whole-cell current recordings revealed that Tef or Tel increased the peak amplitude of  $I_{Na}$ , concomitant with an elevation in the time constant of  $I_{Na}$  inactivation, particularly in the slow component. Conversely, exposure to KB-R7943 resulted in a depression in  $I_{Na}$ , coupled with a decrease in the slow component of the inactivation time constant of  $I_{Na}$ . Theoretical simulations and bifurcation analyses were performed on a modeled interneuron in the spinal dorsal horn. The occurrence of  $I_{Na}$  inactivation accentuated the subthreshold oscillations (SO) in the membrane potential. With an increase in applied current, SO became more pronounced, accompanied by the emergence of high-frequency spiking (HS) with a frequency of approximately 150 Hz. Moreover, an elevation in  $I_{Na}$  conductance further intensified both SO and HF. Consequently, through experimental and in silico studies, this work reflects that Tef, Tel, or KB-R7943 significantly impacts the magnitude and gating properties of  $I_{Na}$  in neurons associated with pain signaling. The alterations in  $I_{Na}$  magnitude and gating in these neurons suggest a close relationship with pain transmission.

**Keywords:** tefluthrin; telmisartan; KB-R7943; voltage-gated Na<sup>+</sup> current; gating kinetics; subthreshold oscillation; high-frequency spiking; bifurcation analysis



**Citation:** Huang, H.-Y.; Huang, Y.-B.; Wu, C.-L.; Wu, S.-N. Modulatory Impact of Tefluthrin, Telmisartan, and KB-R7943 on Voltage-Gated Na<sup>+</sup> Currents. *Biophysica* **2024**, *4*, 488–506. <https://doi.org/10.3390/biophysica4040032>

Academic Editor: Morten Gram Pedersen

Received: 30 August 2024

Revised: 1 October 2024

Accepted: 8 October 2024

Published: 12 October 2024



**Copyright:** © 2024 by the authors. Licensee MDPI, Basel, Switzerland. This article is an open access article distributed under the terms and conditions of the Creative Commons Attribution (CC BY) license (<https://creativecommons.org/licenses/by/4.0/>).

## 1. Introduction

It is established that nine isoforms, specifically Na<sub>v</sub>1.1–1.9 (or SCN1A–SCN5A and SCN8A–SCN11A), of voltage-gated Na<sup>+</sup> (Na<sub>v</sub>) channels are distributed in mammalian excitable tissues, encompassing the central or peripheral nervous system, as well as the endocrine or neuroendocrine system [1–4]. These Na<sub>v</sub> channel proteins in eukaryotes have a single subunit, each containing four six-transmembrane pseudodomains [3].

Upon rapid depolarization, Na<sub>v</sub> channels, which encode macroscopic voltage-gated Na<sup>+</sup> currents ( $I_{Na}$ ), undergo swift transitions from the resting (closed) state to the open state. Subsequently, there is a rapid shift to the inactivated state of the channel [1,2]. The inactivation of  $I_{Na}$  can also accumulate before being triggered during repetitive brief

depolarizing pulses [4–7]. Once evoked, the increased magnitude of  $I_{Na}$  can depolarize the cell membrane through a positive feedback cycle, thereby eliciting the upstroke of the action potentials (APs) and governing the amplitude, frequency, and/or pattern of AP firing in different excitable cells such as sensory neurons [1,2,4].

Tefluthrin (Tef) is a synthetic type-I pyrethroid insecticide that is characterized by the presence of a cyano group at the  $\alpha$ -position of the alcohol moiety. It is recognized as an activator of  $I_{Na}$  and a slowing in current inactivation [8,9]. Permethrin or  $\lambda$ -cyhalothrin, another pyrethroid, has been previously noticed to influence pain signaling [10,11]. Telmisartan (Tel) is a medication belonging to the class of angiotensin II receptor blockers. Despite its primary therapeutic effects on cardiovascular function, there is some evidence to reflect that Tel has additional effects on pain signaling [12]. Whether the presence of Tef or Tel alters the amplitude and gating kinetics of  $I_{Na}$  in sensory or dorsal root ganglion (DRG) neurons is unclear. Alternatively, KB-R7943, an inhibitor of  $Na^+$ - $Ca^{2+}$  exchange process [13,14], has been reported to cause an antinociceptive effect in the neuropathic pain model [15,16]. However, notably, how KB-R7943 can cause any perturbations on  $I_{Na}$  linked to nociceptive signaling is unknown.

Although Tef is classified as a pyrethroid insecticide, Tel acts as a blocker of angiotensin II receptors, and KB-R7943 inhibits  $Na^+$ - $Ca^{2+}$  exchange process, it remains unclear how these three compounds regulate neuronal firing associated with pain signaling.

Therefore, the primary aim of this study was to examine the impact of three compounds—Tef, Tel, and KB-R7943—on cultured DRG neurons. Specifically, the investigation focused on determining whether and how these compounds affect the magnitude and gating kinetics of  $I_{Na}$ . Additionally, a computational model of an interneuron, originally derived from the spinal dorsal horn [17], was utilized to investigate the influence of variations in  $I_{Na}$  inactivation and conductance, both individually and in combination, on dynamic changes in membrane potential. This investigation also employed the generation of bifurcation diagrams [18–20].

## 2. Materials and Methods

### 2.1. Chemicals, Reagents, and Solutions Used in This Study

KB-R7943 (2-[2-[4-(4-nitrobenzyloxy)phenyl]ethyl]isothioureia, 2-[4-[(4-nitrophenyl)methoxy]phenyl]ethyl ester carbamimidiothioic acid,  $C_{16}H_{17}N_3O_3S \cdot CH_3SO_3H$ ) was acquired from Cayman (Excel Biomedical, Tainan, Taiwan). Ranolazine (Ranexa<sup>®</sup>, CV Therapeutics, Palo Alto, CA, USA) and Tel (Micardis<sup>®</sup>, Boehringer Ingelheim, Germany) were supplied by Tocris (Bristol, UK), while Tef, tetraethylammonium chloride (TEA), and tetrodotoxin (TTX) were by Sigma-Aldrich (St. Louis, MO, USA). The stock solutions of Tef, Tel, and KB-R7943 were prepared at a concentration of 10 mM and stored at  $-20^\circ C$  until use.

The extracellular solution, specifically HEPES-buffered normal Tyrode's solution, had the following compositions (mM): NaCl 136.5, KCl 5.4,  $CaCl_2$  1.8,  $MgCl_2$  0.53, glucose 5.5, and HEPES 5.5 (pH 7.4). In order to assess macroscopic  $K^+$  currents or membrane potential, we utilized a recording electrode filled with a solution containing the following (in mM): K-aspartate 130, KCl 20,  $MgCl_2$  1,  $Na_2ATP$  3,  $Na_2GTP$  0.1, EGTA 0.1, and HEPES 5 m (pH 7.2). For recording  $I_{Na}$ ,  $K^+$  ions within the intracellular solution were substituted with equimolar  $Cs^+$  ions, and the pH was then adjusted to 7.2 with CsOH.

### 2.2. Cell Preparation

The rat DRG neurons (neonatal) were a high-quality sensory neuron suspension acquired from Lonza Walkersville, Inc. (R-DRG-505; Walkersville, MD, USA) available at [https://bioscience.lonza.com/lonza\\_bs/TW/en/document/27607](https://bioscience.lonza.com/lonza_bs/TW/en/document/27607) (accessed on 15 July 2024). Following the recommended conditions, the cells were cultured using the PNBMTM BulletKitTM (Lonza, Basel, Switzerland), which includes a 200 mL bottle of primary neuron basal medium (PNBMTM) and PNGMTM SingleQuotsTM. The dorsal horn of the spinal cord was isolated from Sprague–Dawley rat embryos at embryonic day 15–17. The cells were dissociated using mechanical trituration and enzyme digestion, followed by suspension in

minimal essential medium. The cells were incubated at 37 °C in monolayer cultures within a humidified environment containing 5% CO<sub>2</sub>/95% air. Experiments were conducted five or six days after subculturing the cells, at a confluence of 60–80%. Experimental protocols were consistent with ethical principles for animal research approved by the Institutional Animal Care and Use Committee of National Cheng Kung University.

### 2.3. Electrophysiological Measurements

Before the experiments, we dispersed DRG neurons using a 1% trypsin/EDTA solution. A small volume of cell suspension was transferred to a specially crafted chamber affixed on the stage of an inverted microscope. Cells were bathed at room temperature (20–25 °C) in the standard Tyrode's solution. Prior to each measurement, the cells were allowed to settle at the chamber's bottom. The patch pipettes were fashioned from Kimax<sup>®</sup>-51 borosilicate glass tube (#DWK34500-99; Kimble<sup>®</sup>, VWR Scientific, West Chester, PA, USA) and polished to attain a resistance ranging between 2 and 4 MΩ. Recordings of  $I_{Na}$  or other ionic currents were conducted in the whole-cell mode using a modified patch-clamp technique, employing an RK-400 amplifier (Bio-Logic, Claix, France) [21].

To nullify liquid junction potentials resulting from disparities between the composition of the pipette solution and that of the bath, adjustments were made before giga-Ω formation, and subsequent corrections were applied to the whole-cell data. The capacitive transients induced during  $I_{Na}$  elicitation were counteracted by applying a hyperpolarizing pulse of equal magnitude. Cell-membrane capacitance of 28–49 pF ( $37.3 \pm 5.6$  pF;  $n = 29$ ) was compensated. Figure 1 illustrates a histogram showing the relationship between cell number and cell capacitance.

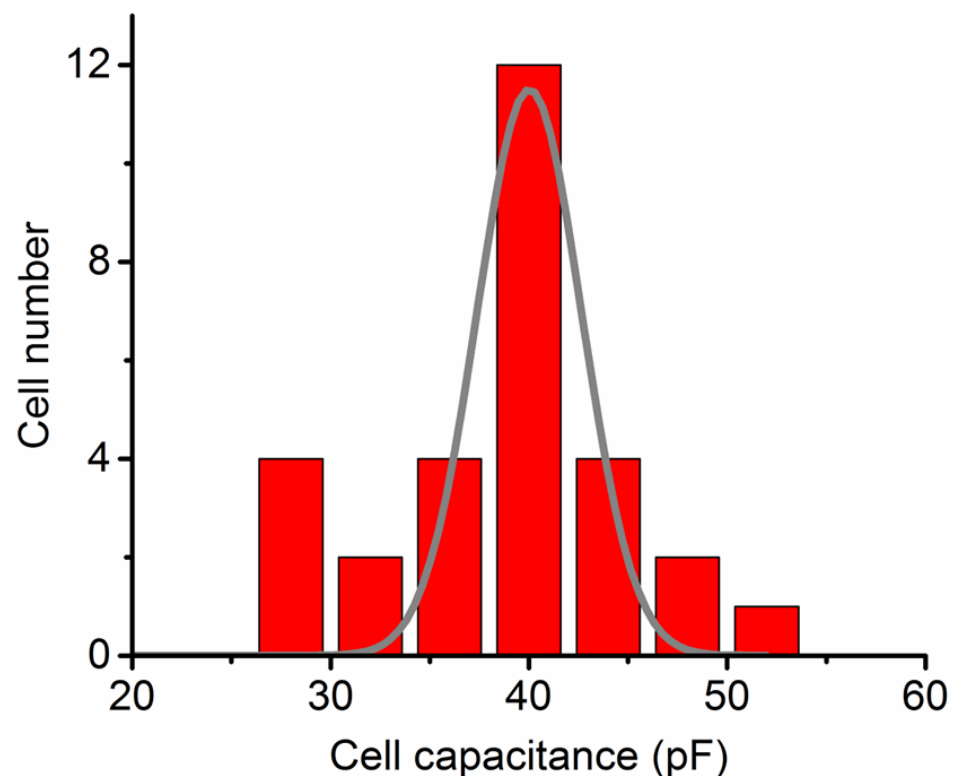


**Figure 1.** Histogram depicting the relationship between cell number and cell capacitance. Each red bar represents the number of cells used in this study. A smooth line overlaid on the histogram illustrates the Gaussian distribution used for curve fitting.

#### 2.4. Data Recordings

The data were stored online on a laptop computer at 5 kHz or higher. The computer was equipped with Digidata<sup>®</sup> 1440A device (Molecular Devices, Forest City, CA, USA), facilitating analog-to-digital and digital-to-analog conversions controlled by pCLAMP<sup>®</sup> 10.6 (Molecular Devices). Offline analyses of the acquired signals were performed using various analytical tools, including OriginPro<sup>®</sup> 2021 (OriginLab, Northampton, MA, USA), and custom-made macros developed in Excel<sup>®</sup> 2022 (Redmond, WA, USA).

#### 2.5. Curve-Fitting Procedures for $I_{Na}$ Inactivation Time Course

The decay of the inactivation time course of  $I_{Na}$  is elucidated through a family of exponential functions. This family can be defined as

$$y(t) = \sum_{i=1}^n A_i \times \exp\left(-\frac{t}{\tau_i}\right)$$

Here,  $y(t)$  symbolizes the inactivation trajectory of  $I_{Na}$  over time, and the index  $i$  commonly takes on two values corresponding to the fast and slow components in the observed inactivation of  $I_{Na}$ . The nonlinear curve-fitting was performed to extract the parameters for the fast ( $\tau_{\text{inact(F)}}$ ) and slow component ( $\tau_{\text{inact(S)}}$ ) of the inactivation time constant ( $\tau_{\text{inact}}$ ).

#### 2.6. Statistical Analyses

The experimental results are expressed as the means  $\pm$  SEM with sample sizes ( $n$ ) indicating the cell number from which the data were taken. The paired or unpaired Student's  $t$ -test and one- or two-way analysis of variance (ANOVA) followed by post hoc Fisher's least-significant difference test were made for the evaluation of differences among means. Statistical analyses were performed using IBM SPSS Statistics 24.0 (Armonk, New York, NY, USA). The significance was determined at a  $p$  value of  $<0.05$ .

#### 2.7. Computer Simulations

To explore the influence of changes in the amplitude and/or inactivation characteristics of  $I_{Na}$  on the AP firing related to pain signaling, we utilized a theoretical model of AP firing derived previously [17]. This model is based on the biophysical properties of parvalbumin-expressing interneurons (PVINs) situated within the dorsal horn of the spinal cord. Voltage-gated  $Ca^{2+}$  current with concurrent changes in intracellular  $Ca^{2+}$  concentrations ( $[Ca^{2+}]_i$ ) were also included in the model [17,22]. The detailed descriptions of the modeled neuron were provided previously [17]. The mathematical model is given by the following:

$$\left\{ C_m \cdot \frac{dV}{dt} = -I_{Na} - I_K - I_A - I_{KDR} - I_{leak} + I_{app} \dot{x} = \frac{x_{\infty} - x}{\tau_x}, x = m_{Na}, h_{Na}, n_K, n_A, I_A, n_{KDR}, h_{KDR} \right\}$$

To simulate changes in the rate of  $I_{Na}$  inactivation, we mathematically constructed a modified Hodgkin–Huxley (HH) type model. The detailed framework utilized in this work was previously described [17], and the biophysical characteristics of  $I_{Na}$  were noted to closely resemble those from earlier studies [23,24]. For  $I_{Na}$ , the modified HH scheme was used according to the following equation:

$$I_{Na} = g_{Na} \times m_{\infty}^3 \times h \times (V - V_{Na})$$

The rate constants for  $I_{Na}$  activation used in the simulation are described by the following equations [17,25]:

$$m_{\infty} = \frac{1}{1 + \exp\left(\frac{V+17.5}{-11.4}\right)}$$

The inactivation variable  $h$  in the paper of Ma et al. (2023) satisfies the dynamic equation

$$\frac{dh}{dt} = \alpha_h \cdot (1 - h) - \beta_h \cdot h,$$

where

$$\alpha_h = \frac{0.0025}{\exp\left(\frac{V-23}{10}\right)}$$

$$\beta_h = \frac{0.094 \cdot (V + 31)}{1 - \exp\left(\frac{V+31}{-5.5}\right)}$$

Moreover, an arbitrarily incorporated adjustable  $\beta_h$ -inactivation parameter of  $I_{Na}$ , represented as  $\varnothing$ , was integrated into the simulated neuron to mimic how variations in the inactivation time course of  $I_{Na}$  and current conductance ( $g_{Na}$ ) can influence the patterns of subthreshold oscillation (SO) or AP firing. This, in turn, leads to modifications in the bifurcation diagram through AUTO implementation [18–20,26].

In particular, the inactivation parameter of  $I_{Na}$  used for mimicking the increase or decrease in current inactivation is reformulated by

$$\frac{dh}{dt} = \alpha_h \cdot (1 - h) - \varnothing \cdot \beta_h \cdot h$$

where  $h$  is inactivation gating variable,  $\alpha_h$  and  $\beta_h$  are the rate constants for inactivation gating variable, and the parameter  $\varnothing$  represents the magnitude of  $Na_V$ -channel inactivation embedded in the  $\beta_h$  inactivation component. As the value of  $\varnothing$  is decreased, the time course of  $Na_V$  channel inactivation elicited by membrane depolarization becomes slowed.

For detailed information on other ionic currents involved in simulated changes in membrane potential, such as voltage-gated  $Ca^{2+}$  current,  $K_V1.3$   $K^+$  current,  $K_V3.1$   $K^+$  current, and small-conductance  $Ca^{2+}$ -activated  $K^+$  current., please refer to the previous work by Ma et al. [17].

## 2.8. Numerical Simulation Technique Employed in This Study

The XPPAUT simulation package, accessible at <https://sites.pitt.edu/~phase/bard/bardware/xpp/xpp.html> (accessed on 27 December 2023), was utilized to conduct analyses related to linear stability and bifurcation. The term “bifurcation” refers to points in parameter space where the system undergoes a qualitative change in its dynamics, leading to the emergence of new solutions or the alteration of existing ones [18,26]. XPPAUT 8.0, a software tool for simulating and analyzing dynamical systems, provides a platform for conducting bifurcation analyses. The AUTO function in XPPAUT refers to a utility within the software that is used for bifurcation analysis [18–20,26].

## 3. Results

### 3.1. Effects of Either Tef, Tel, or KB-R7943 on $I_{Na}$ Measured from Rat DRG Neurons

The initial series of experiments aimed to explore the possible impact of Tef, Tel, or KB-R7943 on  $I_{Na}$  elicited in response to short step depolarizations in these cells. The cells were bathed in  $Ca^{2+}$ -free Tyrode's solution supplemented with 0.5 mM  $CdCl_2$  and 10 mM TEA. The whole-cell voltage-clamp experiments were conducted using a pipette solution containing  $Cs^+$ . As shown in Figure 2, the tested cell was depolarized from  $-100$  to  $-10$  mV for 30 ms, and the  $I_{Na}$ , which was sensitive to block by TTX (1  $\mu$ M), could be readily elicited in these neurons. As shown in Figure 2A, further addition of TTX (1  $\mu$ M) completely blocks the  $I_{Na}$  amplitude observed during continued exposure to 10  $\mu$ M Tef.

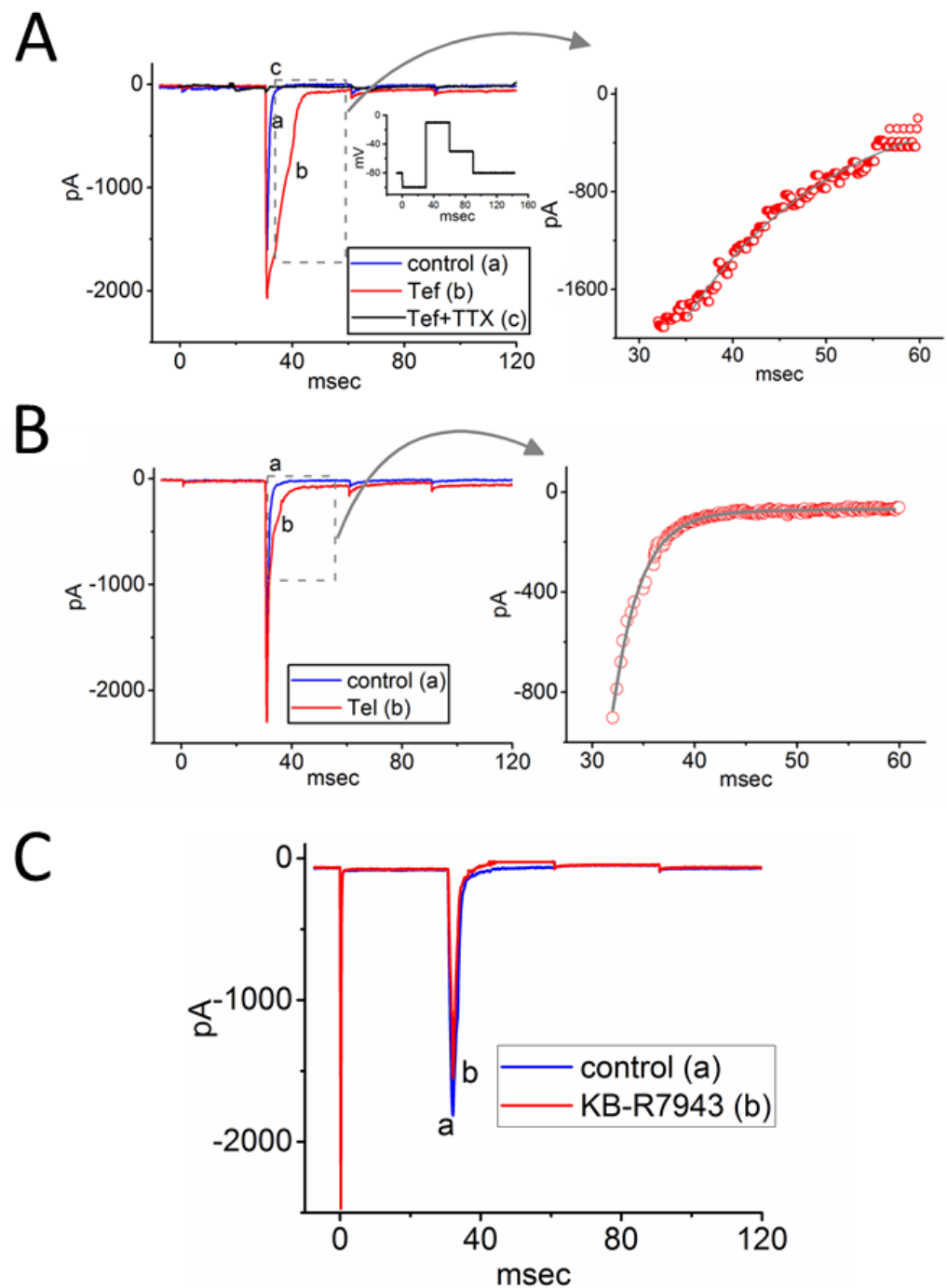


**Figure 2.** Effects of tefluthrin (Tef), telmisartan (Tel), and KB-R7943 on voltage-gated  $\text{Na}^+$  current ( $I_{\text{Na}}$ ) in rat dorsal root ganglion (DRG) neurons using whole-cell current recordings. These experiments were conducted in  $\text{Ca}^{2+}$ -free Tyrode's solution containing  $\text{CdCl}_2$  (0.5 mM) and tetraethylammonium chloride (TEA, 10 mM). Panel (A–C) displays  $I_{\text{Na}}$  traces under the conditions: in the absence (a, blue color) and in the presence (b, red color) of Tef (10  $\mu\text{M}$ ), Tel (10  $\mu\text{M}$ ), or KB-R7943 (10  $\mu\text{M}$ ), respectively. Inset in the left side of panel (A) indicates the voltage-clamp protocol applied. The right graph of panels (A,B) shows an expanded view of the dashed box from the left side, with the red data points fitted to a two-exponential function (gray curve). Please note that in panel (A), the current trace labeled c (black color) indicates further addition of tetrodotoxin (TTX, 1  $\mu\text{M}$ ), in the continued presence of Tef (10  $\mu\text{M}$ ).

Exposure to Tef or Tel exhibited an enhancement in the peak amplitude of  $I_{Na}$ , accompanied by a progressive slowing of the inactivation time course of the current (Figure 2A,B). For example, during a step depolarization from  $-100$  to  $-10$  mV, the addition of Tef ( $10 \mu\text{M}$ ) or Tel ( $10 \mu\text{M}$ ) increased the peak  $I_{Na}$  amplitude from  $1.3 \pm 0.3$  to  $2.4 \pm 0.8$  nA ( $n = 8$ , paired  $t$ -test,  $df = 7$ ,  $p = 0.019$ ) or from  $1.1 \pm 0.3$  to  $2.2 \pm 0.9$  nA ( $n = 8$ , paired  $t$ -test,  $df = 7$ ,  $p = 0.032$ ), respectively. After washout of Tef or Tel,  $I_{Na}$  amplitude returned to the control level. Additionally, during cell exposure to  $10 \mu\text{M}$  Tef or  $10 \mu\text{M}$  Tel, the slow component of the inactivation time constant of  $I_{Na}$  ( $\tau_{\text{inact(S)}}$ ) was prolonged, shifting from  $10.6 \pm 1.8$  to  $23.6 \pm 2.1$  ms ( $n = 8$ , paired  $t$ -test,  $df = 7$ ,  $p = 0.021$ ) and from  $12.2 \pm 2.0$  to  $22.4 \pm 2.1$  ms ( $n = 8$ , paired  $t$ -test,  $df = 7$ ,  $p = 0.024$ ), respectively. However, the value in the fast component of the inactivation time constant ( $\tau_{\text{inact(F)}}$ ) obtained in the presence of Tef or Tel was not changed ( $1.3 \pm 0.3$  ms [control],  $1.4 \pm 0.4$  ms [in the presence of Tef], and  $1.4 \pm 0.3$  ms [in the presence of Tel];  $n = 8$ , one-way ANOVA,  $df_{\text{between}} = 2$ ,  $df_{\text{within}} = 21$ ,  $p = 0.069$ ). Furthermore, when cells were exposed to  $10 \mu\text{M}$  KB-R7943, the peak  $I_{Na}$  amplitude decreased, accompanied by a concurrent reduction in the  $\tau_{\text{inact(S)}}$  value of the current (Figure 2C). The presence of  $10 \mu\text{M}$  KB-R7943 significantly decreased the peak  $I_{Na}$  amplitude from  $1.76 \pm 0.05$  to  $1.51 \pm 0.04$  nA ( $n = 8$ , paired  $t$ -test,  $df = 7$ ,  $p = 0.028$ ). Concurrently, the value of  $\tau_{\text{inact(S)}}$  decreased from  $6.1 \pm 0.2$  to  $2.1 \pm 0.1$  ms ( $n = 8$ , paired  $t$ -test,  $df = 7$ ,  $p = 0.030$ ). However, the  $\tau_{\text{inact(F)}}$  value obtained with or without the KB-R7943 presence remained unaltered. We isolated neurons from the dorsal horn of the spinal cord in rats and found that Tef enhanced the  $I_{Na}$  amplitude. When cells were exposed to Tef ( $10 \mu\text{M}$ ), the peak amplitude of  $I_{Na}$  increased from  $0.45 \pm 0.02$  to  $0.67 \pm 0.03$  nA ( $n = 6$ , paired  $t$ -test,  $df = 5$ ,  $p = 0.039$ ). Additionally, the inactivation time constant ( $\tau_{\text{inact(S)}}$ ) increased from  $4.5 \pm 0.1$  to  $8.9 \pm 0.2$  ms ( $n = 6$ , paired  $t$ -test,  $df = 5$ ,  $p = 0.021$ ).

### 3.2. Simulated $I_{Na}$ Traces Created from a Modified HH Model

In our endeavor to replicate the impact of Tef, Tel, or KB-R7943 on  $I_{Na}$  in cultured DRG neurons, we undertook a detailed exploration into the modulation of both  $I_{Na}$  amplitude and gating. This work aimed to elucidate the influence on the electrical properties of neurons related to nociceptive signaling. The  $I_{Na}$  model employed in these simulations was developed based on a modified HH model [17,20,27,28]. In this series of simulations, the values of  $g_{Na}$  and  $V_{Na}$  were set to be  $120$  nS and  $+58$  mV, respectively. Other parameters are outlined in Table 1 and in a recent paper [17].

**Table 1.** Default parametric values used for the modeling of interneurons in the dorsal horn of the spinal cord. For more detailed parameters of this model, please refer to Ma et al. [17].

Symbol or Parameter	Description *	Value
$C_m$	Membrane capacitance (pF)	30
$g_{Na}$	Maximum $\text{Na}^+$ current conductance (nS)	300
$g_{Ca}$	Maximum $\text{Ca}^{2+}$ current conductance (nS)	8
$g_{K1}$	Maximum $\text{K}_V1$ current conductance (nS)	15
$g_{K3}$	Maximum $\text{K}_V3$ current conductance (nS)	180
$g_{SK}$	Maximum SK $\text{K}^+$ current conductance (nS)	10
$g_{\text{leak}}$	Maximum leak current conductance (nS)	8
$V_{Na}$	$\text{Na}^+$ reversal potential (mV)	58
$V_K$	$\text{K}^+$ reversal potential (mV)	$-80$
$V_{Ca}$	$\text{Ca}^{2+}$ reversal potential (mV)	68
$V_{\text{Leak}}$	Reversal potential for leak current (mV)	$-50$
$\gamma$	$\text{Ca}^{2+}$ recovery rate ( $\text{ms}^{-1}$ )	0.01
$k_{SK}$	$\text{Ca}^{2+}$ sensitivity of SK channel ( $\mu\text{M}$ )	0.8
$A$	Cell surface area ( $\mu\text{m}^2$ )	3000
$\emptyset$	Adjustable $\beta_h$ -inactivation parameter of $h$ gating variable (dimensionless)	1.0

\* The unit of each parameter is indicated in parentheses.

Under the specified conditions, when the  $\varnothing$  value, particularly within the  $\beta_h$  inactivation component of  $h$  inactivation variable, was increased in a stepwise fashion, the inactivation time course of the simulated  $I_{Na}$  progressively became enhanced. This was accompanied by a reduction in the late component of  $I_{Na}$  during rapid step depolarization. It is established that a stepwise increase of the  $\varnothing$  value (from 0.4 to 1.2) embedded in  $h$  inactivation variable is capable of increasing the inactivation rate of the current with a reduction in the sustained component of  $I_{Na}$  (Figure 3), although the amplitude in the transient component of the current was slightly changed. Therefore, the simulated  $I_{Na}$  trajectories within this modeled neuron aligned closely well with the experimentally observed results, showing that the presence of Tef, Tel, or KB-R7943 altered the inactivation time course of this current in cultured DRG neurons (Figure 2).

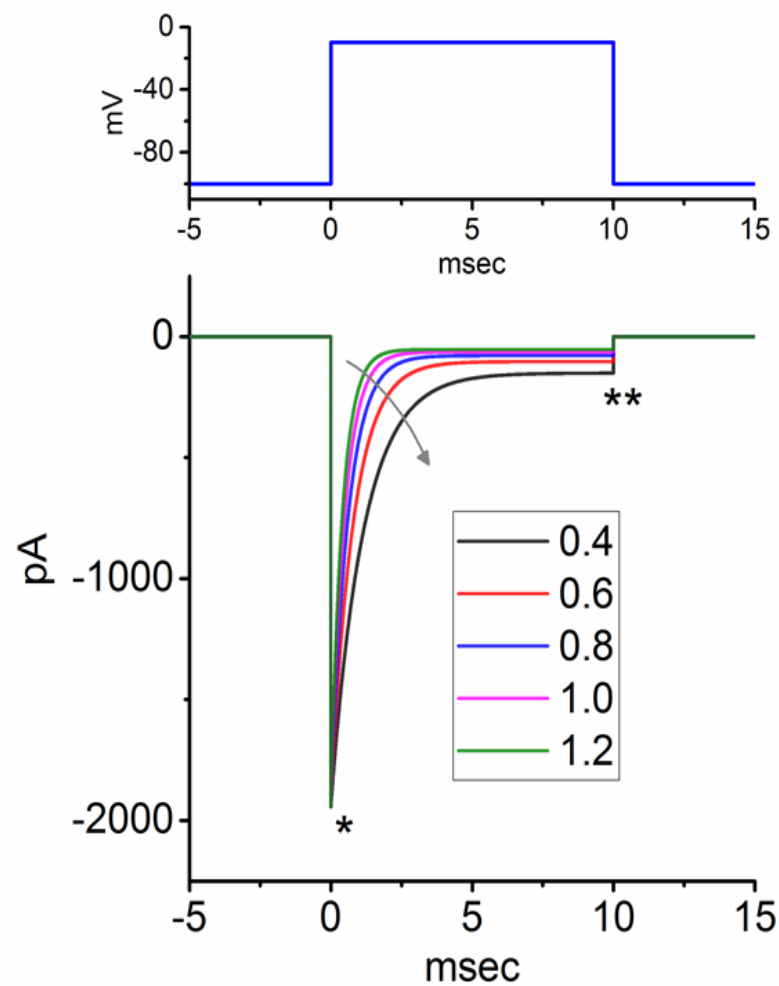


**Figure 3.** Simulated  $I_{Na}$  traces in response to short depolarization from  $-100$  to  $-10$  mV for 10 ms. A detailed profile is described in the Section 2 and in a previous paper (Ma et al., 2023) [17].  $I_{Na}$  traces were created when the  $\varnothing$  value in the inactivation process ( $\beta_h$ ) of  $h$  variable decreased from 1.2 to 0.4 with 0.2 decrements (as indicated by curved arrow). The term " $\beta_h$ " in the HH kinetics refers to the rate at which the  $Na_V$  channel undergoes inactivation in the  $h$  gating variable. \* and \*\* represent the transient and late components of  $I_{Na}$  activated by an abrupt depolarizing pulse. The upper part illustrates the voltage-clamp protocol applied.

### 3.3. Changes of Membrane Potential Caused by Different Value of $\varnothing$

The variations in membrane potential resulting from different  $\varnothing$  values were further investigated. In Figure 4A,  $\varnothing$  was set at 1.0, with  $g_{Na}$  and the applied current ( $I_{app}$ ) set at 400 nS and 300 pA, respectively, and the resulting changes in membrane potential were plotted over time. Under these simulations, a transient oscillatory spike followed by



subthreshold oscillations (SOs) was observed. Notably, the amplitude and frequency of APs exhibited progressive decreases, indicative of spike-frequency adaptation [29,30]. The emergence of SOs, as previously observed in interior olive neurons [13], was evident.

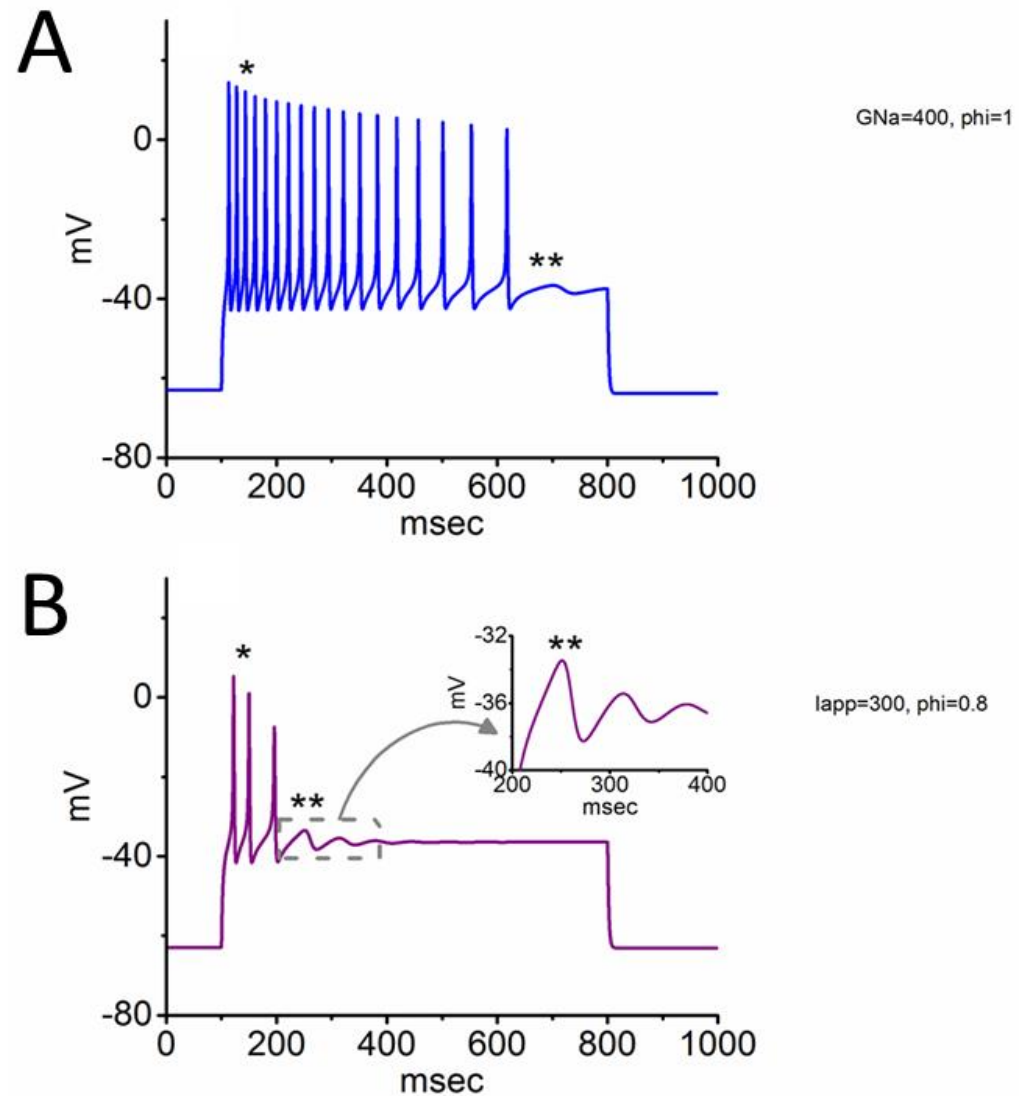


**Figure 4.** Two distinct spiking patterns simulated from the modeled neuron. When a current injection (700 ms in duration) was applied to this modeled neuron, two different spike patterns emerged, namely, somatic spike (SS) and subthreshold oscillation (SO). In panel (A),  $g_{Na} = 400$  nS,  $I_{app} = 300$  pA,  $\varphi = 1.0$ . In panel (B),  $g_{Na} = 300$  nS,  $I_{app} = 300$  pA,  $\varphi = 0.8$ . The symbols \* and \*\* represent the occurrence of SS and SO, respectively. The inset in panel (B) is a magnified view from the dashed box in (B), highlighting the SO emergence.

However, when the  $g_{Na}$  value was decreased to 300 nS while maintaining the same values for  $I_{app}$  and  $\varphi$ , both the amplitude and frequency of APs in response to current injection were reduced. Following the cessation of APs, the occurrence of SO was also observed (Figure 4B). Findings from these results highlight that changes in  $g_{Na}$  alone can alter the electrical behavior of the modeled neurons.

### 3.4. Relationship of Changes in Steady-State Membrane Potential vs. the $I_{app}$ Value

In this study, a bifurcation analysis was employed to explore alterations in the steady-state membrane potential in response to variations in the  $I_{app}$ . A bifurcation diagram is a graphical representation of the long-term behavior of a dynamical system as a parameter is changed [13,18,20]. Through these simulations,  $I_{app}$  was considered a variable, while other parameters were maintained at default values (Table 1). With a constant value of  $\emptyset$  set to 1, Figure 5 depicts the bifurcation diagram illustrating the correlation between  $I_{app}$  and the change in membrane potential. Two critical values of  $I_{app}$ , representing the subcritical and supercritical bifurcation points, were identified. Specifically, the  $I_{app}$  values for these points at  $\emptyset = 1$  were noted to be 88 and 177 pA. Within the range of  $I_{app}$  values between these two Hopf bifurcation points, a stable limit cycle emerged—a closed trajectory in the phase plane, indicating the SO occurrence in the modeled neuron, as demonstrated previously [13,18]. The range of membrane potential changes were found to be between  $-39.3$  and  $-36.2$  mV. The model therefore exhibits stability when  $I_{app}$  is below the subcritical point or above the supercritical point. Conversely, self-sustained periodic oscillations, or SOs, occur when  $I_{app}$  falls within the range between the subcritical and supercritical points.

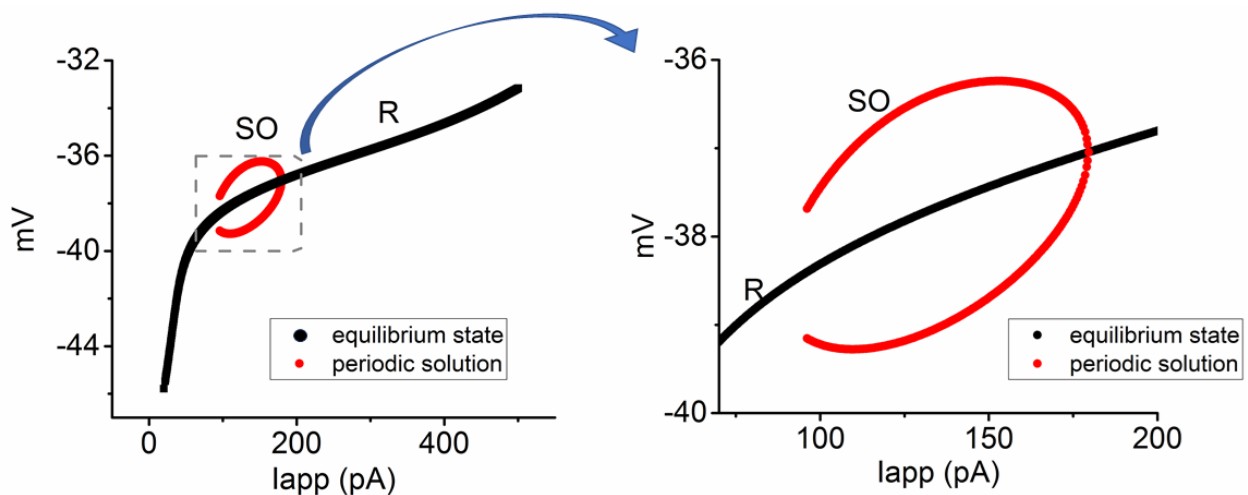


**Figure 5.** Bifurcation diagram illustrating the relationship between  $I_{app}$  and alterations in membrane potential in the modeled neuron. These simulations were conducted using default parameters detailed in Table 1, with a  $\emptyset$  value of 1.0. Two types of solutions in the system were identified. That is, one is the resting, steady-state, or equilibrium state (R, black color), while the other is the unstable and periodic solution indicative of SO (red color). The enlarged graph on the (right) corresponds to the highlighted region within the dashed box on the (left).

However, a notable alteration in the bifurcation diagram occurred when the  $\emptyset$  value in the  $\beta_h$  inactivation process of  $h$  inactivation variable decreased to 0.8 with a fixed  $g_{Na}$  value of 300 nS, mimicking a slowing in the inactivation time course of  $I_{Na}$  (Figure 6A,B). Under these conditions, two types of periodical solutions were observed. The subcritical and supercritical points, determining the occurrence of preexisting SO, increased to 95 and 367 pA, respectively. Additionally, another phenomenon, namely, somatic spiking (SS) or somatic AP firing, was noted during the existence of  $I_{app}$  ranging between 52 and 98 pA. Within the domain of SS, the voltage of membrane potential was found to range between  $-40$  and  $+15$  mV. It is also noted from Figure 6B that as the SO domain overlapped with SS, the cell behavior was denoted to be SS/SO bistable in the system, when the  $I_{app}$  amplitude ranged between 79 and 118 pA.

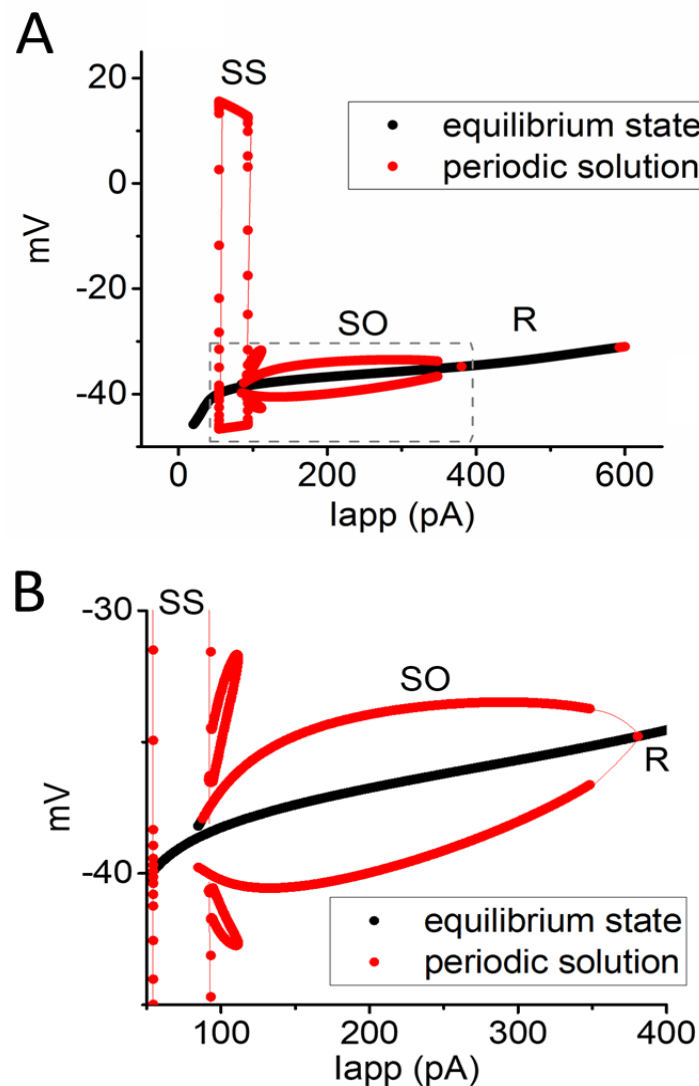


**Figure 6.** Bifurcation diagram concerning the relationship between  $I_{app}$  and membrane potential in the modeled neuron with a constant  $\varnothing$  value of 0.8. Beside the equilibrium or resting state (R, in black color), two distinct types of periodic solutions (indicated in red color) were identified, namely, SS occurring within the  $I_{app}$  range of 52 to 97 pA and SO at the  $I_{app}$  range between 85 and 381 pA. Panel (B) is an enlarged view of the dashed box in panel (A).

### 3.5. Further Modifications on Changes in Membrane Potential with the Increasing $I_{app}$ Value with a Fixed $\varnothing$ Value of 0.8

We made further adjustments to investigate how an additional large increase in  $I_{app}$  amplitude, with the fixed  $\varnothing$  and  $g_{Na}$  values of 0.8 and 300 nS, influences changes in membrane potential,  $I_{Na}$ , and intracellular  $Ca^{2+}$  levels ( $[Ca^{2+}]_i$ ) in the modeled neuron. As depicted in Figure 7A–C, setting the  $I_{app}$  value of 700 pA resulted in high-frequency spiking (HS) of APs at a rate of 150 Hz. The membrane potential during this HS spiking exhibited periodical fluctuations with the range of  $-39$  to  $+18$  mV. Moreover, when HS occurred, the height of the AP gradually decreased over time, accompanied by a reduction of  $I_{Na}$  amplitude. This phenomenon corresponds to previous experimental reports, showing an accumulation of  $I_{Na}$  inactivation when excitable cells are subjected to high-frequency depolarizing stimuli [5–7,31]. Alternatively, the  $[Ca^{2+}]_i$  level rose during AP firing. Over the 700 ms duration of  $I_{app}$ , the  $[Ca^{2+}]_i$  level concurrently increased from 1.11 to 1.42  $\mu$ M.

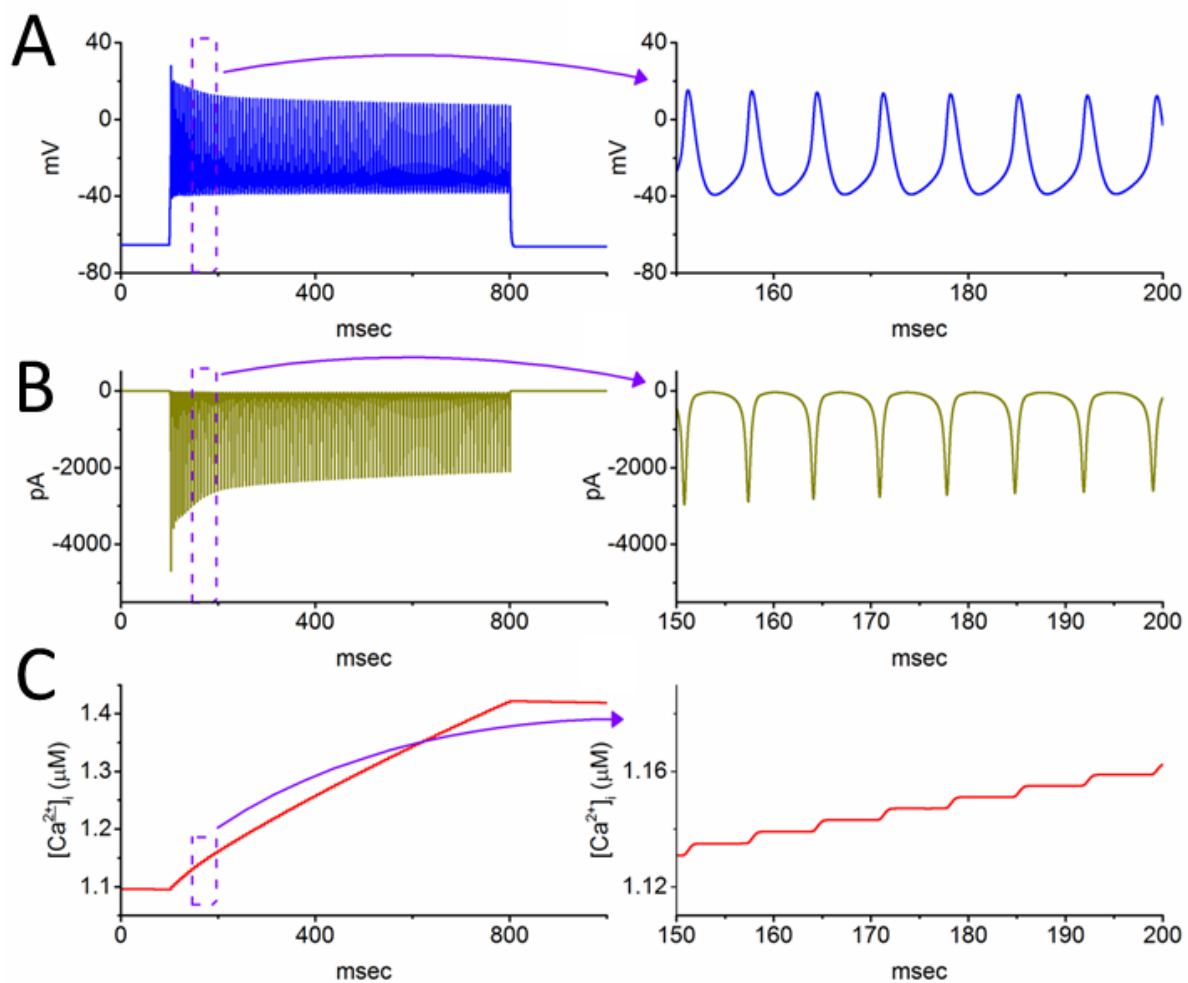


**Figure 7.** Effect of elevated  $I_{app}$  at 700 pA on spiking,  $I_{Na}$ , and intracellular  $Ca^{2+}$  concentration ( $[Ca^{2+}]_i$ ) in the simulated neuron. Panels (A–C), respectively, depict membrane potential,  $I_{Na}$  amplitude, and  $[Ca^{2+}]_i$  induced by a 700 ms  $I_{app}$  with 700 pA. Each corresponding panel on the right provides an enlarged view of the graph contained within the dashed box on the left.

### 3.6. Bifurcation Analysis on the Relationship between $I_{app}$ and Membrane Potential at the Range between 0 and 1200 pA

As demonstrated in Figure 8, the bifurcation diagram, which illustrates the relationship between  $I_{app}$  magnitude and membrane potential, was further examined. Three distinct periodic solutions, highlighted in red, are evident within the system. In these simulations, with  $g_{Na}$  set at 300 nS and  $\varnothing$  at 0.8, a gradual increase in  $I_{app}$  amplitude within the 560 to 910 pA range leads to another self-sustained periodic solution of the system. That is, there appeared to be another closed trajectory in this phase plane. This result indicates the emergence of HS, with a rate reaching 150 Hz (Figure 8). Notably, when both the inactivation time course of  $I_{Na}$  slowed down and the amplitude of  $I_{app}$  were concurrently increased within the range of 560 to 910 nA, the modeled neuron became more predisposed to generate HS, namely, high-frequency firing of APs. Changes in membrane potential were noted to range between  $-35$  and  $+4$  mV during the HS occurrence in the bifurcation diagram. It is thus noted that as the  $g_{Na}$  value increased to 400 nS, the range of limit cycles generated by both SO and HS was observed to increase. Moreover, the pattern of SO was noticeably amalgamated with that of HS, as observed in Figure 9, in comparison to the bifurcation diagram in Figure 8. Therefore, simulated alterations in both the  $I_{Na}$  amplitude and the inactivation time course of the current, as observed experimentally in the presence of Tef or Tel, makes the membrane potential susceptible to SO occurrence and even the HS emergence. Additionally, as found during cell exposure to KB-R7943, both the decrease in

$I_{Na}$  amplitude and the inactivation time course of this current are anticipated to diminish the emergence of SO or HS.

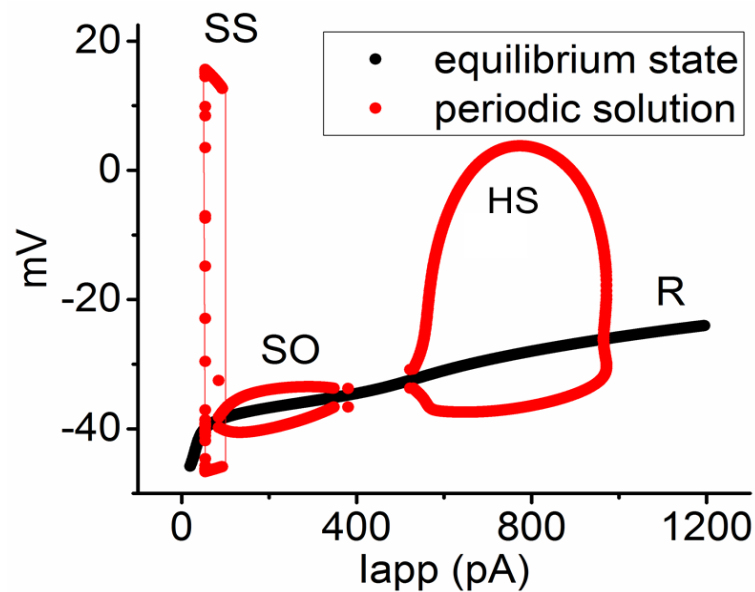


**Figure 8.** Bifurcation diagram showing the relationship between the applied current ( $I_{app}$ ) and membrane potential in the modeled neuron. The parameters were set at  $g_{Na} = 300$  nS and  $\phi = 0.8$ , with the  $I_{app}$  range spanning from 20 to 1300 pA. Three unstable bifurcations (indicated in red color) occur, namely, SS with low frequency, SO, and a high-frequency spiking pattern (HS). This caption suggests that in the presence of compounds like Tef or Tel, the modeled neuron exhibited HS occurrence, especially at higher intensities of applied current ranging between 500 and 950 pA. Red and black colors in this and the following figures denote the periodic solutions (SS, SO, and HS) and the equilibrium or resting state (R), respectively.

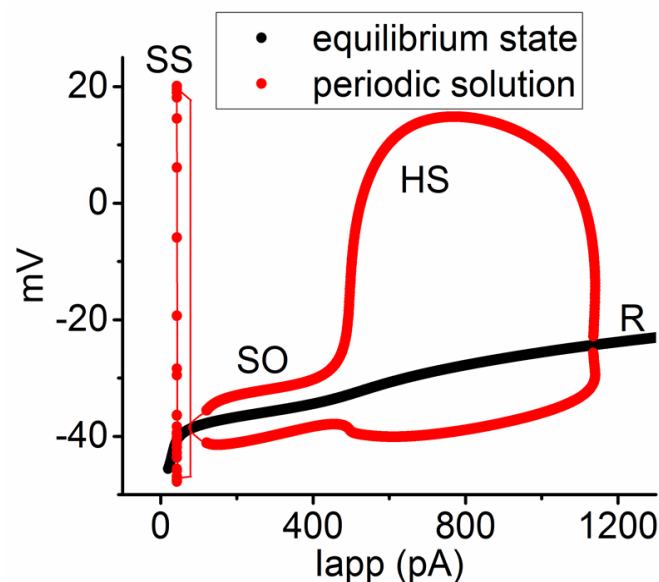


**Figure 9.** Phase diagram illustrating the impact of enhanced  $g_{Na}$  coupled with a reduced  $\phi$  on the relationship of  $I_{app}$  vs. membrane potential. In this diagram, we set  $\phi = 0.8$ , and increased  $g_{Na}$  to 320 nS. With the increased  $I_{app}$ , the coalescence of SO and HS became evident. No existence in the stable steady-state for  $I_{app}$  ranging between 20 and 1100 pA was noted.

#### 4. Discussion

The results of this study demonstrate that in the presence of Tef, Tel, or KB-R7943, the amplitude and gating of  $I_{Na}$  in cultured DRG neurons (R-DRG-505) was affected. Tef or Tel increased the amplitude of  $I_{Na}$  while slowing down the inactivation time course of this current. The impact of Tel on  $I_{Na}$  is related to its effect on  $Na_V$  channels and is not associated with its antagonistic action against angiotensin II receptors [12,20]. Furthermore, in addition to suppression of the  $Na^+-Ca^{2+}$  exchanging process [1,32], KB-R7943 also inhibited the magnitude of  $I_{Na}$  while simultaneously accelerating the inactivation rate of  $I_{Na}$  in cultured DRG neurons.

This study shows that the presence of  $I_{Na}$  can be detected in cultured DRG neurons. However, these  $I_{Na}$  currents are blocked by TTX. In these cells, we did not observe clear TTX-resistant (TTX-R)  $I_{Na}$  [33,34]. The  $Na_V1.6$ ,  $Na_V1.7$ ,  $Na_V1.8$ , and  $Na_V1.9$  isoforms were noticed to be expressed in DRG neurons. It is thus possible that the  $Na_V1.8$  expression in these cells (R-DRG-505 cells) could be relatively low [35]. However, we did observe that the current was enhanced by Tef or Tel and inhibited by KB-R7943, as reported previously [20,36–39]. Additionally, the inactivation time course of these currents was also altered by these drugs (Figure 2). Our *in silico* study proposed that the inactivation time course of  $I_{Na}$  (indicated by the variable  $\phi$  value), which is activated at depolarized potentials, contributes to the presence, amplitude, and frequency of SO and HS [4,13,18,34].

In the modeled interneuron of this study, there were no parameters for the  $Na^+-Ca^{2+}$  exchanging process. However, with the generation of AP firing, the level of  $[Ca^{2+}]_i$  also increased, as demonstrated in Figure 6. Therefore, at least in excitable cells such as neuronal cells, changes in the magnitude of  $I_{Na}$  or the inactivation time course of the current might affect the level of  $[Ca^{2+}]_i$  without the need for the participation of the  $Na^+-Ca^{2+}$  exchanging process. Indeed, KB-R7943, an inhibitor of the  $Na^+-Ca^{2+}$  exchanging process [14,15], was reported to inhibit the  $I_{Na}$  responsible for these effects [21].

Previous reports have indicated that ranolazine, a blocker of late  $I_{Na}$ , has an inhibitory effect on the  $I_{Na}$  in DRG neurons, concurrently demonstrating relief in painful sensations [23,40,41]. This study confirms this phenomenon and additionally reveals that KB-R7943, an inhibitor of the  $Na^+-Ca^{2+}$  exchanging process, can inhibit  $I_{Na}$  magnitude while accelerating the inactivation time course of the  $I_{Na}$ , as described recently [21]. Therefore, KB-R7943 may alleviate a certain type of pain signaling [25]. Furthermore, further investigations are needed to explore how Tef or Tel influences the biophysical properties of  $I_{Na}$  in DRG neurons or sensory neurons associated with pain signaling, consequently modulating the nociceptive transmission [10,11,42,43].

The results of this study demonstrate that when the  $I_{Na}$  in DRG neurons increased and its inactivation time course simultaneously slowed down, as mimicked by the presence of Tef or Tel, the cell membrane of these neurons became prone to generating the occurrence of SO. Moreover, excessive stimulation with strong electrical currents easily induced the HS emergence. Conversely, when  $I_{Na}$  decreased and the inactivation time course accelerated (as mimicked by cell exposure to KB-R7943), these cells were less likely to exhibit the pattern of SOs and even resulted in the HS development [13,17,18,28]. Therefore, alterations in the biophysical properties of  $I_{Na}$  impact the cell excitability of DRG neurons *in vivo*, subject to biophysical, pharmacological, or toxicological modulation of  $I_{Na}$ .

The modeled neuron used in this study includes two types of different delayed-rectifier  $K^+$  currents, namely,  $K_V1.3$  and  $K_V3.1$  currents [17]. Previous reports have indicated that changes in the magnitude and inactivation process of these  $K^+$  currents significantly impact the HS emergence [44–48]. KCNQ channels have been also reported to enable reliable presynaptic spiking occurring at high frequency [49]. Therefore, further investigations are needed to understand how the modulation of these  $K^+$  currents may have effects on the HS emergence in the presence of Tef or Tel.

In this study, we employed a theoretical model of AP firing, which was adapted from a previous study by Ma et al. [17]. This model is based on the biophysical properties of PVINs located in the dorsal horn of the spinal cord. Although there are some differences

between this model neuron and the DRG neuron, both of these types of neurons contain abundant  $\text{Na}_V$  channels. We thus believe that it is valuable to investigate how changes in the amplitude and/or inactivation characteristics of  $I_{\text{Na}}$  affect the patterns of AP firing related to pain signaling. However, the effects of these compounds on the AP firing in DRG neurons occurring *in vivo* still require further analysis and research.

Although our study found that TTX-R  $I_{\text{Na}}$  was not detected in cultured DRG neurons (R-DRG-505), it is established that nociceptive DRG neurons ( $\leq 30 \mu\text{m}$  in a diameter) express TTX-R  $\text{Na}_V$  channels, such as  $\text{Na}_V1.8$  and  $\text{Na}_V1.9$ , and that previous studies have emphasized the role of these channels in nociceptive transmission [35,50,51]. However, the modified PVINs in lamina III of the spinal cord are very heterogeneous and mainly express  $\text{Na}_V1.1$ ,  $\text{Na}_V1.2$ , and  $\text{Na}_V1.6$ , and they do not express  $\text{Na}_V1.7$  abundant in nociceptive DRG neurons [52–54]. Nevertheless, the effects of three compounds on TTX-R  $\text{Na}_V$  channels should be tested, possibly using native DRG neurons or other types of spinal neurons linked to pain transmission.

Plasma Tel concentration after intravenous administration of a single dose of 40 mg Tel was noted to reach about  $2.32 \mu\text{M}$  [55]. As for Tel, it is a pyrethroid insecticide. Its concentration in the blood of organisms varies greatly, reaching up to several micromolar levels. After intravenous administration, KB-R7943 reached a concentration of about  $0.12 \mu\text{M}$  [56], which is lower than the concentration used in this study. However, recent reports have found that KB-R7943 can cross the blood–brain barrier, with concentrations in brain tissue reaching 5 to 10 times higher [16].

The effects of these compounds on the dorsal root ganglia may extend beyond the necessity of the blood–brain barrier. However, in nociceptive transmission, the dorsal root ganglia is one of the first primary neurons; the nerve transmission also needs to reach the dorsal horn of the spinal cord, then pass and conduct through long fibers upward to the medulla oblongata, further up to the thalamus, and then to the cerebral cortex. In these regions, the blood–brain barrier is often present. Therefore, if these compounds, such as TelTef or KB-7943, can easily pass through the blood–brain barrier across those areas, it is believed that they could have a regulatory effect on these pain-linked transmission pathways. Furthermore, neurons of the dorsal horn of the spinal cord, including parvalbumin-expressing interneurons, were reported to exhibit greater heterogeneity than DRG neurons [54]. Nevertheless, the effects of Tel, Tef, or KB-R7943 may have implications for biological activity in the nervous system [8,9]. Among these effects, the regulation of ion channels in the cell membrane might be one of the important mechanisms.

Of note, the model used in the current study is not perfect. Indeed, there are many different formulations for  $\text{Na}^+$  currents. The simulated firing of neuronal action potentials derived from different regions linked to pain signaling can also be present in various possible forms, as detailed on the ModelDB website (<http://modeldb.sicence/>, accessed on 14 July 2024).

To ensure our experimental results are more substantial and effective in presentations, and to observe potential action potential firing patterns, we further explored this through bifurcation analysis. We indeed spent a significant amount of time searching for developments of various types of simulation models. Thus, we found the model developed by Ma et al. [17] in PVINs to be more suitable for our needs. However, we still believe it is not perfect, and in the future, we will continue to develop more suitable computational models so that the experimentally observed and theoretical results can be more consistent.

Tef has previously been reported to inhibit voltage-gated  $\text{Ca}^{2+}$  current and mildly suppress delayed-rectifier  $\text{K}^+$  currents [57]. Additionally, telmisartan has been shown to suppress *erg*-mediated  $\text{K}^+$  currents [37]. However, there are no reports indicating that KB-R7943 affects  $\text{K}^+$  currents. This paper focuses solely on the changes these compounds induce in the amplitude and gating of  $\text{Na}^+$  currents. Further analysis is required to understand the effects of these agents on other ion currents, such as  $\text{K}^+$  and  $\text{Ca}^{2+}$  currents, is necessary. Therefore, additional research is necessary to provide further clarification in this area.

**Limitation of study.** In our cultured DRG neurons, namely, R-DRG-505 cells, we employed current-clamp voltage recordings to observe changes in membrane potential. However, we were unable to detect HS. Even in the presence of Tef or Tel, HS did not manifest. However, through our investigations using modeled interneurons in the spinal dorsal horn [17], we found that enhancing the  $I_{Na}$  and slowing down the inactivation time course can simulate the exposure to Tef or Tel. The simulations suggest that these modeled neurons can generate SO and HS. Furthermore, when subjected to strong applied currents, HS with a rate of about 150 Hz was found to emerge. The theoretical analyses of these scenarios are presented in the bifurcation diagrams provided herein.

Additionally, to induce differentiation-like events in cell culture and observe variable AP firing patterns, the medium might be replaced with one containing 1  $\mu$ M nerve growth factor. The experimental and theoretical observations in this study may serve as a foundation for future research aimed in these directions. Furthermore, the concentrations used in this research project are very close to the potential clinical, pharmaceutical, or toxicological application ranges of these compounds. Therefore, the research findings will hold practical significance for the appropriate administration or use of these compounds.

**Author Contributions:** Conceptualization, H.-Y.H., C.-L.W. and S.-N.W.; Methodology, Y.-B.H. and S.-N.W.; Validation, Y.-B.H.; Formal analysis, Y.-B.H. and S.-N.W.; Investigation, H.-Y.H.; Data curation, C.-L.W.; Writing—original draft, C.-L.W.; Writing—review and editing, S.-N.W.; Supervision, S.-N.W.; Project administration, C.-L.W.; Funding acquisition, H.-Y.H. All authors have read and agreed to the published version of the manuscript.

**Funding:** This work was partly supported by grants from the Ministry of Science and Technology (NSTC-113-2923-B-906-001), Taiwan, from An Nan Hospital (ANHR-112-42, ANHR-112-43, and ANHR-112-44), and Ditmanson Medical Foundation Chia-Yi Christian Hospital Research Program. The funders were not involved in the study, design, data collection, analyses, or interpretation.

**Data Availability Statement:** The data will be made available upon request.

**Acknowledgments:** The authors of this study express gratitude to the late Ching-Hsing Luo of the Department of Electrical Engineering at National Cheng Kung University, Tainan, Taiwan, for his assistance in the earlier work on bifurcation analyses.

**Conflicts of Interest:** The authors declare that the research was conducted in the absence of any commercial or financial relationships that could be construed as potential conflicts of interest.

## Abbreviations

AP, action potential;  $[Ca^{2+}]_i$ , intracellular  $Ca^{2+}$  concentration; df, degree of freedom; HH, Hodgkin-Huxley; HS, high-frequency spiking; DRG neuron, dorsal root ganglion neuron; Iapp, applied current;  $I_{Na}$ , voltage-gated  $Na^+$  current;  $Na_V$  channel, voltage-gated  $Na^+$  channel; SK channel, small-conductance  $Ca^{2+}$ -activated  $K^+$  channel; PVINs, parvalbumin-expressing interneurons; SO, subthreshold oscillation; SS, somatic spiking;  $\tau_{inact(F)}$ , fast component of inactivation time constant;  $\tau_{inact(S)}$ , slow component of inactivation time constant; Tef, tefluthrin; Tel, telmisartan; TTX, tetrodotoxin; TTX-R, tetrodotoxin-resistant. (The other abbreviations related to parameters used in the simulations are detailed in Table 1).

## References

1. Catterall, W.A. Voltage-gated sodium channels at 60: Structure, function and pathophysiology. *J. Physiol.* **2012**, *590*, 2577–2589. [[CrossRef](#)] [[PubMed](#)]
2. De Lera Ruiz, M.; Kraus, R.L. Voltage-Gated Sodium Channels: Structure, Function, Pharmacology, and Clinical Indications. *J. Med. Chem.* **2015**, *58*, 7093–7118. [[CrossRef](#)] [[PubMed](#)]
3. Shen, H.; Zhou, Q.; Pan, X.; Li, Z.; Wu, J.; Yan, N. Structure of a eukaryotic voltage-gated sodium channel at near-atomic resolution. *Science* **2017**, *355*, eaal4326. [[CrossRef](#)]



4. Bennett, D.L.; Clark, A.J.; Huang, J.; Waxman, S.G.; Dib-Hajj, S.D. The Role of Voltage-Gated Sodium Channels in Pain Signaling. *Physiol. Rev.* **2019**, *99*, 1079–1151. [[CrossRef](#)] [[PubMed](#)]
5. Taddese, A.; Bean, B.P. Subthreshold Sodium Current from Rapidly Inactivating Sodium Channels Drives Spontaneous Firing of Tubermammillary Neurons. *Neuron* **2002**, *33*, 587–600. [[CrossRef](#)]
6. Carter, B.C.; Bean, B.P. Incomplete Inactivation and Rapid Recovery of Voltage-Dependent Sodium Channels During High-Frequency Firing in Cerebellar Purkinje Neurons. *J. Neurophysiol.* **2011**, *105*, 860–871. [[CrossRef](#)]
7. Huang, C.-W.; Hung, T.-Y.; Wu, S.-N. The inhibitory actions by lacosamide, a functionalized amino acid, on voltage-gated Na<sup>+</sup> currents. *Neuroscience* **2015**, *287*, 125–136. [[CrossRef](#)]
8. So, E.C.; Wu, S.-N.; Lo, Y.-C.; Su, K. Differential regulation of tefluthrin and telmisartan on the gating charges of I<sub>Na</sub> activation and inactivation as well as on resurgent and persistent I<sub>Na</sub> in a pituitary cell line (GH<sub>3</sub>). *Toxicol. Lett.* **2018**, *285*, 104–112. [[CrossRef](#)]
9. Lin, M.-H.; Lin, J.-F.; Yu, M.-C.; Wu, S.-N.; Wu, C.-L.; Cho, H.-Y. Characterization in Potent Modulation on Voltage-Gated Na<sup>+</sup> Current Exerted by Deltamethrin, a Pyrethroid Insecticide. *Int. J. Mol. Sci.* **2022**, *23*, 14733. [[CrossRef](#)]
10. Jiang, N.; Nutter, T.J.; Cooper, B.Y. Molecular and cellular influences of permethrin on mammalian nociceptors at physiological temperatures. *NeuroToxicology* **2013**, *37*, 207–219. [[CrossRef](#)]
11. Silwal, P.M.; Adhikari, R.; Yadav, B.M.; Sah, S.K.M.; Bhatt, A.; Basnet, S.M. Lambda-cyhalothrin ingestion: An infrequent yet concerning presentation of pyrethroid poisoning. *Ann. Med. Surg.* **2023**, *85*, 5250–5254. [[CrossRef](#)] [[PubMed](#)]
12. Hegazy, N.; Rezaq, S.; Fahmy, A. Renin-angiotensin system blockade modulates both the peripheral and central components of neuropathic pain in rats: Role of calcitonin gene-related peptide, substance P and nitric oxide. *Basic Clin. Pharmacol. Toxicol.* **2020**, *127*, 451–460. [[CrossRef](#)] [[PubMed](#)]
13. Schweighofer, N.; Doya, K.; Kawato, M.; Davoine, F.; Curti, S.; Hakimian, S.; Norris, S.A.; Greger, B.; Keating, J.G.; Anderson, C.H.; et al. Electrophysiological properties of inferior olive neurons: A compartmental model. *J. Neurophysiol.* **1999**, *82*, 804–817. [[CrossRef](#)] [[PubMed](#)]
14. Amran, S.; Homma, N.; Hashimoto, K. Pharmacology of KB-R7943: A Na<sup>+</sup>-Ca<sup>2+</sup> exchange inhibitor. *Cardiovasc. Drug Rev.* **2003**, *21*, 255–276. [[CrossRef](#)]
15. Huang, Y.; Wen, L.-L.; Xie, J.-D.; Ouyang, H.-D.; Chen, D.-T.; Zeng, W.-A. Antinociceptive effectiveness of the inhibition of NCX reverse-mode action in rodent neuropathic pain model. *Mol. Pain* **2019**, *15*, 1744806919864511. [[CrossRef](#)]
16. Andreeva-Gateva, P.; Hristov, M.; Strokova-Stoilova, M.; Ivanova, N.; Sabit, Z.; Surcheva, S.; Beliakov, M.; Karakashev, G.; Sukhov, I.; Belinskaya, D.; et al. Therapeutic potential of orally applied KB-R7943 in streptozotocin-induced neuropathy in rats. *Heliyon* **2024**, *10*, e27367. [[CrossRef](#)] [[PubMed](#)]
17. Ma, X.; Miraucourt, L.S.; Qiu, H.; Sharif-Naeini, R.; Khadra, A. Modulation of SK Channels via Calcium Buffering Tunes Intrinsic Excitability of Parvalbumin Interneurons in Neuropathic Pain: A Computational and Experimental Investigation. *J. Neurosci.* **2023**, *43*, 5608–5622. [[CrossRef](#)]
18. White, J.; Budde, T.; Kay, A. A bifurcation analysis of neuronal subthreshold oscillations. *Biophys. J.* **1995**, *69*, 1203–1217. [[CrossRef](#)]
19. Enns-Ruttan, J.S.; Miura, R.M. Spontaneous Secondary Spiking in Excitable Cells. *J. Theor. Biol.* **2000**, *205*, 181–199. [[CrossRef](#)]
20. Chang, T.-T.; Yang, C.-J.; Lee, Y.-C.; Wu, S.-N. Stimulatory Action of Telmisartan, an Antagonist of Angiotensin II Receptor, on Voltage-Gated Na<sup>+</sup> Current: Experimental and Theoretical Studies. *Chin. J. Physiol.* **2018**, *61*, 1–13. [[CrossRef](#)]
21. Wu, S.-N.; Yu, M.-C. Inhibition of Voltage-Gated Na<sup>+</sup> Currents Exerted by KB-R7943 (2-[2-[4-(4-nitrobenzyloxy)phenyl]ethyl]isothiourea), an Inhibitor of Na<sup>+</sup>-Ca<sup>2+</sup> Exchanging Process. *Int. J. Mol. Sci.* **2023**, *24*, 1805. [[CrossRef](#)] [[PubMed](#)]
22. Brown, A.M. A modeling study predicts the presence of voltage gated Ca<sup>2+</sup> channels on myelinated central axons. *Comput. Methods Programs Biomed.* **2002**, *71*, 25–31. [[CrossRef](#)] [[PubMed](#)]
23. Wu, S.-N.; So, E.C.; Liao, Y.-K.; Huang, Y.-M. Reversal by ranolazine of doxorubicin-induced prolongation in the inactivation of late sodium current in rat dorsal root ganglion neurons. *Pain Med.* **2015**, *16*, 1032–1034. [[CrossRef](#)]
24. Ghovanloo, M.-R.; Tyagi, S.; Zhao, P.; Effraim, P.R.; Dib-Hajj, S.D.; Waxman, S.G. Sodium currents in naïve mouse dorsal root ganglion neurons: No major differences between sexes. *Channels* **2023**, *18*, 2289256. [[CrossRef](#)]
25. Traub, R.D.; Miles, R. Multiple Modes of Neuronal Population Activity Emerge after Modifying Specific Synapses in a Model of the CA3 Region of the Hippocampus. *Ann. N. Y. Acad. Sci.* **1991**, *627*, 277–290. [[CrossRef](#)]
26. Winslow, R.L. Bifurcation analysis of nonlinear retinal horizontal cell models. I. Properties of isolated cells. *J. Neurophysiol.* **1989**, *62*, 738–749. [[CrossRef](#)] [[PubMed](#)]
27. Wu, S.-N. Simulations of the cardiac action potential based on the Hodgkin-Huxley kinetics with the use of Microsoft Excel spreadsheets. *Chin. J. Physiol.* **2004**, *47*, 15–22.
28. Chen, B.-S. Effects of Transient Receptor Potential-Like Current on the Firing Pattern of Action Potentials in the Hodgkin-Huxley Neuron during Exposure to Sinusoidal External Voltage. *Chin. J. Physiol.* **2010**, *53*, 423–429. [[CrossRef](#)] [[PubMed](#)]
29. Chiesa, N.; Rosati, B.; Arcangeli, A.; Olivetto, M.; Wanke, E. A Novel Role for HERG K<sup>+</sup> Channels: Spike-Frequency Adaptation. *J. Physiol.* **1997**, *501*, 313–318. [[CrossRef](#)]
30. Wu, S.; Yeh, C.; Huang, H.; So, E.C.; Lo, Y. Electrophysiological characterization of sodium-activated potassium channels in NG108-15 and NSC-34 motor neuron-like cells. *Acta Physiol.* **2012**, *206*, 120–134. [[CrossRef](#)]

31. A Navarro, M.; Salari, A.; Lin, J.L.; Cowan, L.M.; Penington, N.J.; Milesu, M.; Milesu, L.S. Sodium channels implement a molecular leaky integrator that detects action potentials and regulates neuronal firing. *eLife* **2020**, *9*, e54940. [[CrossRef](#)] [[PubMed](#)]
32. Schröder, U.H.; Breder, J.; Sabelhaus, C.F.; Reymann, K.G. The novel Na<sup>+</sup>/Ca<sup>2+</sup> exchange inhibitor KB-R7943 protects CA1 neurons in rat hippocampal slices against hypoxic/hypoglycemic injury. *Neuropharmacology* **1999**, *38*, 319–321. [[CrossRef](#)] [[PubMed](#)]
33. Roy, M.; Narahashi, T. Differential properties of tetrodotoxin-sensitive and tetrodotoxin-resistant sodium channels in rat dorsal root ganglion neurons. *J. Neurosci.* **1992**, *12*, 2104–2111. [[CrossRef](#)] [[PubMed](#)]
34. Lee, H.M.; Kim, H.I.; Shin, Y.K.; Lee, C.S.; Park, M.; Song, J.-H. Diclofenac inhibition of sodium currents in rat dorsal root ganglion neurons. *Brain Res.* **2003**, *992*, 120–127. [[CrossRef](#)] [[PubMed](#)]
35. Szulczyk, B.; Pasiński, M.; Gawlak, M. Prefrontal cortex pyramidal neurons express functional Nav1.8 tetrodotoxin-resistant sodium currents. *Clin. Exp. Pharmacol. Physiol.* **2021**, *49*, 350–359. [[CrossRef](#)]
36. Kim, H.K.; Youm, J.B.; Lee, S.R.; Lim, S.E.; Ko, T.H.; Long, L.T.; Nilius, B.; Won, D.N.; Noh, J.-H.; Ko, K.S.; et al. The angiotensin receptor blocker and PPAR-γ agonist, telmisartan, delays inactivation of voltage-gated sodium channel in rat heart: Novel mechanism of drug action. *Pflügers Arch. Eur. J. Physiol.* **2012**, *464*, 631–643. [[CrossRef](#)]
37. Chang, W.; Wu, S. Activation of voltage-gated sodium current and inhibition of erg-mediated potassium current caused by telmisartan, an antagonist of angiotensin II type-1 receptor, in HL-1 atrial cardiomyocytes. *Clin. Exp. Pharmacol. Physiol.* **2018**, *45*, 797–807. [[CrossRef](#)]
38. Lai, M.-C.; Wu, S.-N.; Huang, C.-W. Telmisartan, an Antagonist of Angiotensin II Receptors, Accentuates Voltage-Gated Na<sup>+</sup> Currents and Hippocampal Neuronal Excitability. *Front. Neurosci.* **2020**, *14*, 902. [[CrossRef](#)]
39. Lu, T.-L.; Wu, S.-N. Investigating the Impact of Selective Modulators on the Renin–Angiotensin–Aldosterone System: Unraveling Their Off-Target Perturbations of Transmembrane Ionic Currents. *Int. J. Mol. Sci.* **2023**, *24*, 14007. [[CrossRef](#)]
40. Gould, H.J.; Soignier, R.D.; Cho, S.R.; Hernandez, C.; Diamond, I.; Taylor, B.K.; Paul, D. Ranolazine Attenuates Mechanical Allodynia Associated with Demyelination Injury. *Pain Med.* **2014**, *15*, 1771–1780. [[CrossRef](#)]
41. Gould, H.J.; Diamond, I. Ranolazine: A potential treatment for refractory neuropathic pain. *J. Neurol. Sci.* **2016**, *369*, 310–311. [[CrossRef](#)] [[PubMed](#)]
42. Castellanos, A.; Andres, A.; Bernal, L.; Callejo, G.; Comes, N.; Gual, A.; Giblin, J.P.; Roza, C.; Gasull, X. Pyrethroids inhibit K2P channels and activate sensory neurons: Basis of insecticide-induced paraesthesias. *Pain* **2017**, *159*, 92–105. [[CrossRef](#)] [[PubMed](#)]
43. Karádi, D.; Galambos, A.R.; Lakatos, P.P.; Apenberg, J.; Abbood, S.K.; Balogh, M.; Kiraly, K.; Riba, P.; Essmat, N.; Szucs, E.; et al. Telmisartan Is a Promising Agent for Managing Neuropathic Pain and Delaying Opioid Analgesic Tolerance in Rats. *Int. J. Mol. Sci.* **2023**, *24*, 7970. [[CrossRef](#)] [[PubMed](#)]
44. Klemic, K.G.; Kirsch, G.E.; Jones, S.W. U-Type Inactivation of Kv3.1 and Shaker Potassium Channels. *Biophys. J.* **2001**, *81*, 814–826. [[CrossRef](#)] [[PubMed](#)]
45. Lin, M.-W.; Wang, Y.-J.; Liu, S.-I.; Lin, A.-A.; Lo, Y.-C.; Wu, S.-N. Characterization of aconitine-induced block of delayed rectifier K<sup>+</sup> current in differentiated NG108-15 neuronal cells. *Neuropharmacology* **2008**, *54*, 912–923. [[CrossRef](#)]
46. Wang, Y.-J.; Lin, M.-W.; Lin, A.-A.; Peng, H.; Wu, S.-N. Evidence for state-dependent block of DPI 201-106, a synthetic inhibitor of Na<sup>+</sup> channel inactivation, on delayed-rectifier K<sup>+</sup> current in pituitary tumor (GH3) cells. *Acta Physiol. Pol.* **2008**, *59*, 409–423.
47. Wu, S.-N.; Chen, B.-S.; Lin, M.-W.; Liu, Y.-C. Contribution of slowly inactivating potassium current to delayed firing of action potentials in NG108-15 neuronal cells: Experimental and theoretical studies. *J. Theor. Biol.* **2008**, *252*, 711–721. [[CrossRef](#)]
48. Hsiao, H.-T.; Wang, J.C.-F.; Wu, S.-N. Inhibitory Effectiveness in Delayed-Rectifier Potassium Current Caused by Vortioxetine, Known to Be a Novel Antidepressant. *Biomedicines* **2022**, *10*, 1318. [[CrossRef](#)]
49. Zhang, Y.; Li, D.; Darwish, Y.; Fu, X.; Trussell, L.O.; Huang, H. KCNQ Channels Enable Reliable Presynaptic Spiking and Synaptic Transmission at High Frequency. *J. Neurosci.* **2022**, *42*, 3305–3315. [[CrossRef](#)]
50. Woolf, C.J.; Ma, Q. Nociceptors—Noxious Stimulus Detectors. *Neuron* **2007**, *55*, 353–364. [[CrossRef](#)]
51. Nascimento de Lima, A.P.; Zhang, H.; Chen, L.; Effraim, P.R.; Gomis-Perez, C.; Cheng, X.; Huang, J.; Waxman, S.G.; Dib-Hajj, S.D. Nav1.8 in small dorsal root ganglion neurons contributes to vincristine-induced mechanical allodynia. *Brain* **2024**, *147*, 3157–3170. [[CrossRef](#)] [[PubMed](#)]
52. Fukuoka, T.; Kobayashi, K.; Noguchi, K. Laminae-specific distribution of alpha-subunits of voltage-gated sodium channels in the adult rat spinal cord. *Neuroscience* **2010**, *169*, 994–1006. [[CrossRef](#)]
53. Petitjean, H.; Pawlowski, S.A.; Fraine, S.L.; Sharif, B.; Hamad, D.; Fatima, T.; Berg, J.; Brown, C.M.; Jan, L.-Y.; Ribeiro-Da-Silva, A.; et al. Dorsal Horn Parvalbumin Neurons Are Gate-Keepers of Touch-Evoked Pain after Nerve Injury. *Cell Rep.* **2015**, *13*, 1246–1257. [[CrossRef](#)] [[PubMed](#)]
54. Gradwell, M.A.; Boyle, K.A.; Browne, T.J.; Bell, A.M.; Leonardo, J.; Reyes, F.S.P.; Dickie, A.C.; Smith, K.M.; Callister, R.J.; Dayas, C.V.; et al. Diversity of inhibitory and excitatory parvalbumin interneuron circuits in the dorsal horn. *Pain* **2021**, *163*, e432–e452. [[CrossRef](#)] [[PubMed](#)]
55. Stangier, J.; Schmid, J.; Türck, D.; Switek, H.; Verhagen, A.; Peeters, P.A.; van Marle, S.P.; Tamminga, W.J.; Sollie, F.A.; Jonkman, J.H. Absorption, metabolism, and excretion of intravenously and orally administered [<sup>14</sup>C]telmisartan in healthy volunteers. *J. Clin. Pharmacol.* **2000**, *40*, 1312–1322. [[CrossRef](#)] [[PubMed](#)]

- 
56. Miyata, A.; Zipes, D.P.; Hall, S.; Rubart, M. KB-R7943 Prevents Acute, Atrial Fibrillation–Induced Shortening of Atrial Refractoriness in Anesthetized Dogs. *Circulation* **2002**, *106*, 1410–1419. [[CrossRef](#)]
  57. Wu, S.-N.; Wu, Y.-H.; Chen, B.-S.; Lo, Y.-C.; Liu, Y.-C. Underlying mechanism of actions of tefluthrin, a pyrethroid insecticide, on voltage-gated ion currents and on action currents in pituitary tumor (GH3) cells and GnRH-secreting (GT1-7) neurons. *Toxicology* **2009**, *258*, 70–77. [[CrossRef](#)]

**Disclaimer/Publisher’s Note:** The statements, opinions and data contained in all publications are solely those of the individual author(s) and contributor(s) and not of MDPI and/or the editor(s). MDPI and/or the editor(s) disclaim responsibility for any injury to people or property resulting from any ideas, methods, instructions or products referred to in the content.